# Tunable Infrared Absorption by Metal Nanoparticles: The Case for Gold Rods and Shells

**Nadine Harris[1], Michael J Ford[1], Paul Mulvaney[2] and Michael B Cortie[1,*]**

[1] Mrs N. Harris, A/Prof M.J. Ford, Prof. M.B. Cortie, Institute for Nanoscale Technology, University of Technology Sydney, Broadway, NSW 2007, Australia
[2] Prof. P. Mulvaney, Chemistry School & Bio21 Institute, University of Melbourne, Parkville, VIC 3010, Australia
* Corresponding author Tel: +61-2-9514-2208 and Email: michael.cortie@uts.edu.au

## Abstract

**Nanoparticles of elements such as Au, Al or Ag have optical extinction cross-sections that considerably surpass their geometric cross-sections at certain wavelengths of light. While the absorption and scattering maxima for nanospheres of these elements are relatively insensitive to particle diameter, the surface plasmon resonance of Au nanoshells and nanorods can be readily tuned from the visible into the infrared by changing the shape of the particle. Here we compare nanoshells and nanorods in terms of their ease of synthesis, their optical properties, and their longer term technological prospects as tunable "plasmonic absorbers". While both particle types are now routinely prepared by wet chemistry, we submit that it is more convenient to prepare rods. Furthermore, the plasmon resonance and peak absorption efficiency in nanorods may be readily tuned into the infrared by an increase of their aspect ratio, whereas in nanoshells such tuning may require a decrease in shell thickness to problematic dimensions.**

## Introduction

In recent years there has been intense interest in precious metal nanoparticles of various shapes due to their useful, or potentially useful, optical properties. In particular, Au and Ag nanoparticles with dimensions in the range of 10 to 100 nm are efficient absorbers of light. At the plasmon resonance frequency the absorption cross-section can be several times that expected from the geometrical cross-section of the particle. Moreover, in this size range only limited scattering of the incident light occurs [1-8]. In the present Critical Review we focus on the properties of two specific nanoparticle shapes: *nanoshells and nanorods*, Figure 1. These two forms have gained prominence in the last ten years, although they have antecedents going back several decades. Nanoshells and nanorods of Ag and Au have the especially interesting property that their surface plasmon resonances can be readily tuned across the visible and near-infrared regions of the spectrum. For this reason, decorative [9, 10], diagnostic [11-13], architectural [14, 15], analytical [5, 16], and therapeutic [17-23] applications have recently been proposed for these particles. Of course, Au and Ag *nanospheres* have been known for far longer, having been used for over two thousand years [24]. Spheres, however, are limited in respect of the

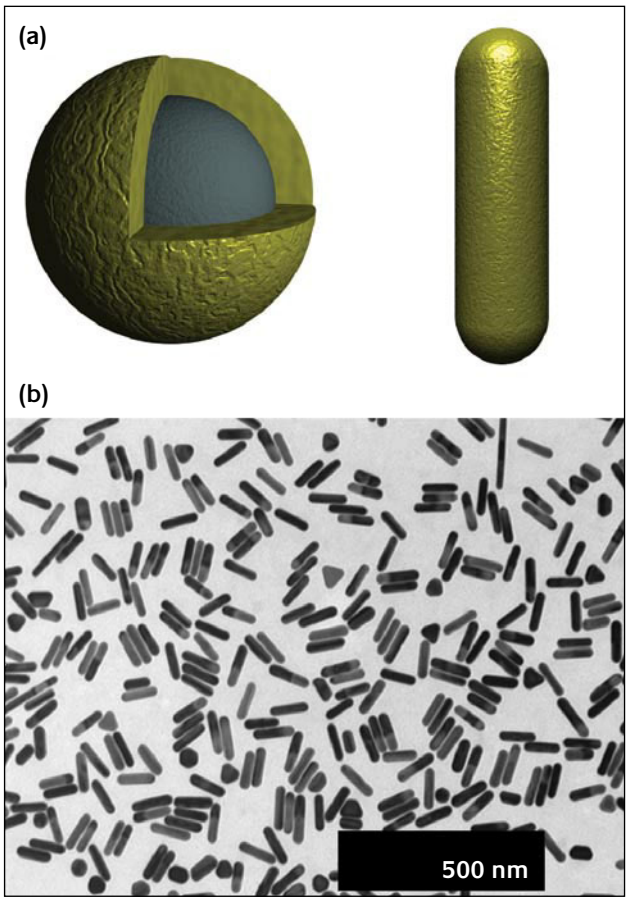


**Figure 1**
*Tunable plasmonic absorbers, A) schematic illustrations of gold nanoshell on dielectric core (left) and gold nanorod (right), B) gold nanorods prepared with the assistance of Ag additions to the growth solution*

tunability of the wavelength at which maximum absorption occurs [25]. The plasmon resonance for Au spheres with diameters between 5 nm and 50 nm is nearly independent of size. This is because the gradient of the real part of the dielectric function, at the plasmon resonance, is large, and the size-dependent shift in the plasmon resonance is inversely proportional to this gradient [26]. For particles smaller than about 5 nm, scattering of electrons off the surface [7, 27] causes a significant decrease in the resonance amplitude, plus a broadening and slight blue shift in its position. For particles larger than about 50 nm there is also a shift in the resonance peak as higher-order terms begin to contribute to the extinction, but with an attendant loss of spectral selectivity. Therefore, neither of these effects provides a convenient method for tuning the resonance peak. Of course, the resonance wavelength of nanospheres can be tuned to some extent by changing the dielectric constant of the medium in which it is embedded [7], a phenomenon that can be exploited for chemical analysis [24, 28-31] or by changing the composition of the sphere itself [2, 32].

The relative merits of rods and shells as absorbers and scatterers of light for medical and biological applications have been analyzed by Jain *et al.* [25], who concluded that Au nanorods were an order of magnitude more effective than nanoshells in terms of absorption and extinction when compared on the basis of overall particle volume. However, the high value of Au implies that a more relevant figure-of-merit will be based on the amount of Au contained per particle, which in the case of nanoshells with their dielectric cores, is a rather different measure. In this article, we directly compare the extinction cross-sections of Au rods and shells in terms of moles of Au used, in order to establish which particles are the better tunable plasmonic, infrared absorbers. This is a fundamental and important criterion for optimizing the design of nanoscale materials in diverse fields such as photothermal therapy, passive solar absorption and heat rejection filters.

## 2 Optical Properties and Synthesis of Nanoshells and Nanorods

### 2.1 Optical Properties of Nanoparticles

Analytical solutions for the optical properties of metal nanospheres, nanoshells and small ellipsoids are available. However, there is no generally applicable analytical solution for arbitrary-shaped nanoparticles and it is common to resort to numerical calculations, often based on the discrete dipole approximation (DDA) [33-35]. In this case the particle is simulated by an array of dipoles with polarizability determined by the dielectric function of the appropriate material. In principle the DDA is an exact technique. In practice, however, there are intrinsic approximations introduced by the grid size used, and by the lattice dispersion relation used to relate the polarizability of the grid points to the dielectric function. In addition there are extrinsic approximations associated with the appropriateness of the dielectric function employed. Calculations made using the analytical solutions are orders of magnitude faster than those made with the DDA, and so are preferred if available. In the present work we have used an analytical solution to calculate the optical properties of the nanoshells, and the DDA for the nanorods. The quality of the DDA is determined by the density of the dipole array, and a compromise is sought between accuracy and computational expense. All the DDA calculations presented here are conducted under computational conditions which exceed those recommended by Draine and Flatau [35]. Similarly, the analytical calculations were carried out to a sufficient number of terms to produce fully converged values for these particle sizes. The agreement between DDA calculations using the present computational conditions and the exact Mie theory, was found to be excellent [4, 34, 36]. The accuracy of DDA calculations for Au nanoparticles has also been verified by several other groups [4, 25, 36, 37].

We have employed the bulk dielectric function of Au for both the analytical and the numerical solutions [38]. However, the Drude model for the optical properties of a free electron model states that the real (ε′) and imaginary (ε″) parts of the dielectric function are [2] :

$$\varepsilon' = 1 - \frac{\omega_p^2}{\omega^2 + \gamma^2} \quad (1)$$

$$\varepsilon'' = \frac{\omega_p^2 \gamma}{\omega(\omega^2 + \gamma^2)} \quad (2)$$

where $\omega_p$ is the plasma frequency, $\omega = \frac{2\pi c}{\lambda}$, $c$ the speed of light in a vacuum, $\lambda$ the wavelength of incident light and $\gamma$ the damping constant. Decreasing the size of a nanoparticle will eventually cause the thickness to become less than the bulk mean free path, and electron scattering from the surfaces of the particle will have the effect of decreasing and broadening its plasmon resonance peak(s). There is a correction available for the case of nanoshells and in this case $\gamma$ can be modified to [2]:

$$\gamma = \gamma_{bulk} + \frac{v_F}{r_{eff}} \quad (3)$$

where $\gamma_{bulk}$ is the damping constant for the bulk material, $v_F$ is the electron velocity at the Fermi surface and $r_{eff}$ is the effective mean free path of collisions. The latter can be calculated from [7] :

$$r_{eff} = \frac{\{(d_2 - d_1)(d_2^2 - d_1^2)\}^{\frac{1}{3}}}{2} \quad (4)$$

with $d_1$ the diameter of the inner shell core and $d_2$ the outer shell diameter.

The mean free path for conduction electrons in Au is about 40 nm, so the effective damping frequency ($\omega_f(r) = \omega_f(\infty) + v_F/r$, where $v_F$ is the velocity of electrons at the Fermi energy, and $r$ the mean free path of the conduction electrons) is increased by about a factor of two for particles

of roughly that size. This will broaden the transverse mode of both spheres and rods, and significantly broaden the extinction peaks of shells. However, the longitudinal resonance of rods is hardly affected by surface damping and, indeed, has one of the lowest dephasing times known [39, 40].

Optical extinction, absorption and scattering values are often compared in terms of an efficiency, *Q*. The extinction efficiency, $Q_{ext}$, is the extinction cross-section of the particle normalized to its geometric cross-section. This is a convenient method for spherical particles as it provides an effective parameter against which different size particles can be compared directly. However, for non-spherical particles there is no obvious way of defining the geometric cross-section. The most common convention, at least with computational codes, is to reduce the volume of the particle to an equivalent sphere and use the cross-sectional area of this sphere. This makes sense when extinctions are orientationally averaged, but can hide many of the interesting, shape-dependent effects. In this work we therefore use the absolute absorption and scattering cross-section values and normalize these to the true cross-section of the particle, that is, the cross-sectional area the particle presents to light incident from a particular direction. In addition we compare the absorption for particles containing identical volumes of Au, rather than for particles of equal overall volume (i.e. we exclude the core material in the case of nanoshells). This provides a true, "molar" basis for comparison, which is also an important consideration for any practical application for these particles.

## 2.2 Nanoshells

### *2.2.1 Optical properties*

It has been recognized since at least 1951 that core-shell nanoparticles have versatile optical properties [7, 41-43] although the fact probably only became more widely appreciated after a series of publications [44-46] and patents [47-50] by the group of N. Halas in the USA. These workers also pointed out that Au nanoshells could have diverse medical applications. It was demonstrated that a thin shell of a metal such as Au surrounding a spherical dielectric core exhibits two surface plasmon resonances associated with the outer and inner surfaces of the shell. As the shell thickness is decreased the two surface plasmons will interact with each other more strongly and hence shift in position relative to the position of the individual resonances of the sphere surface or cavity [51]. This effect has been described in terms of hybridization of the two plasmon resonances by analogy to the hybridization of molecular orbitals in quantum chemistry [52]. Clearly, if the shell is made sufficiently thick the cavity resonance is not excited by the incident light and the core-shell particle will approximate a solid sphere. For thin Au shells, however, the interaction of the two plasmons may be exploited to tune the wavelength of peak extinction from the mid-visible into the near-infrared by varying the ratio of the core to shell radius (the 'shell aspect ratio').

Detailed descriptions of the optical properties of nanoshells have been presented elsewhere [2, 41, 42]. Briefly however, an analytical solution is available, and was therefore used here in preference to the DDA. The extinction cross section of the particle within the dipole limit is given by:

$$C_{ext} = k\,\mathrm{Im}(\alpha) \tag{5}$$

where $\alpha$ is the complex polarizability of the particle, the wavenumber $k = 2\pi\frac{\sqrt{\varepsilon_m}}{\lambda}$, $\lambda$ is the wavelength of the incident light *in* vacuo and $\varepsilon_m$ is the dielectric function of the non-absorbing medium in which the particle is embedded. The polarizability of a small coated sphere (shell) can be described in the electrostatic limit ($k_r$<<1) by [2] :

$$\alpha = 4\pi r_2^3 \frac{(\varepsilon_2-\varepsilon_m)(\varepsilon_1+2\varepsilon_2)+f(\varepsilon_1-\varepsilon_2)(\varepsilon_m+2\varepsilon_2)}{(\varepsilon_2+2\varepsilon_m)(\varepsilon_1+2\varepsilon_2)+f(2\varepsilon_2-2\varepsilon_m)(\varepsilon_1-\varepsilon_2)} \tag{6}$$

where $r_2$ is the shell radius, $\varepsilon_1$, $\varepsilon_2$, $\varepsilon_m$ are the dielectric functions of the inner core, outer core and surrounding medium, respectively and $f$ is the fraction of the total particle volume occupied by the core, that is $f = \left(\frac{r_1}{r_2}\right)^3$ with $r_1$ the shell inner core radius. The exact position of the maximum absorption peak within the spectrum is determined by the dielectric functions of the nanoshell and surrounding medium.

Excitation of the fundamental or "Fröhlich" mode [2] follows by setting the denominator of Eqn. 1 to 0:

$$(\varepsilon_2+2\varepsilon_m)(\varepsilon_1+2\varepsilon_2)+f(2\varepsilon_2-2\varepsilon_m)(\varepsilon_1-\varepsilon_2)=0 \tag{7}$$

If we assume that the dielectric function of the surrounding medium is unity, it is possible to write a simple expression for the resonance condition [2]:

$$\varepsilon_1 = -2\varepsilon_2\left[\frac{\varepsilon_2(1-f)+(2+f)}{\varepsilon_2(2f+1)+2(1-f)}\right] \tag{8}$$

It is evident that the magnitude and the position of the plasmon peak within the spectra can be varied by simply varying the aspect ratio and/or the dielectric constant of the core, shell and/or the surrounding medium.

Nanoshell extinction spectra were calculated using the BHCOAT [2] implementation of Mie theory [53], which solves the following equation [42]:

$$Q_{sca} = \left(\frac{2}{\alpha^2}\right)\sum_{n=1}^{\infty}(2n+1)\left(|a_n|^2+|b_n|^2\right) \tag{9}$$

Where $\alpha = \frac{2\pi b}{\lambda}$, $b$ is equal to the radius of the particle, $\lambda$ is the wavelength of incident radiation and $\mathrm{a}_n$ and $\mathrm{b}_n$ are the scattering coefficients, suitably modified for a shell [2].

Eq.9 is the exact solution, in terms of a multi-pole expansion for the scattering cross-section of an arbitrarily sized, spherical core-shell particle. In practice the multi-pole expansion must be truncated at some point; however, for particle sizes in the present work only the first half-dozen terms contribute and the results are therefore essentially exact. While we have used the exact, analytical solution here, this system also provides a useful benchmark for validating the DDA solution. Indeed for core-shell spheres, we find excellent agreement between DDA and eq.9.

The ability to tune the magnitude and position of peak $Q_{ext}$ within the spectra of nanoshells has been demonstrated experimentally, with maximum extinctions readily varied between 600 and 1000 nm [45, 54-57]. The observed peak shift is not unique to Au nanoshells. The criterion for the establishment of this geometry-dependent phenomenon is the existence of a negative real part of the dielectric function of the nanoshell metal within the visible regime. Consequently the peak absorption of nanoshells made from an element such as Ag can also be tuned. This has been demonstrated by Chen and co-workers [58] who synthesized Ag nanoshells with outer diameters of 40 – 50 nm and inner diameters of 20 – 30 nm. They observed a resonant peak at 395 nm for a 20 nm diameter solid Ag particle (in comparison to the peak at ~520 nm for a similarly sized Au nanoparticle). However, when these particles were transformed into shells the resonant peak red-shifted to 506 nm, as expected. It is evident, however, that extinction peaks for Ag nanoshells will always be at shorter wavelengths than those for similarly-shaped Au nanoshells due to the manner in which their respective refractive indices vary with wavelength.

The ability to tune the plasmon modes of a nanoshell into the near-infrared is, however, somewhat constrained by two factors. Decreasing the shell thickness well below the electron mean free path causes the resonances to attenuate and broaden as described previously. On the other hand, the alternative solution, keeping the shell thickness constant but increasing the outer diameter will cause a large increase in light scattering and loss of spectral selectivity [59].

#### *2.2.2 Synthesis of nanoshells*

Recognition of the tunable nature of the optical properties of nanoshells has led to attention being focused on methods for producing good quality core-shell nanoparticles using either wet chemical [31, 45, 55, 56] or template-based techniques [60, 61]. At present it is most common to use wet chemistry techniques to produce Au nanoshells. An early and simple method was due to Zhou *et al.* [62] whereby the surface of Au sulfide ($Au_2S$) nanoparticles was reduced to produce a Au layer. However, there has subsequently been more interest in a technique pioneered in the late 1990s by the Halas group in which a template particle is functionalized with some moiety to which Au nanoparticle seeds can subsequently attach. Following this, the seeds are grown so that they coalesce to form a continuous shell. Oldenburg *et al.* [45] produced silica-Au core-shell particles with diameters of around 120 nm this way by functionalizing the surface of the silica cores with 3-aminopropyltriethoxysilane (APS), and then partially covering the surface with 1 – 2 nm Au particles that were covalently bound to the APS. After this, the silica particles, with their partial Au covering, behave as nucleation sites for the reduction of $HAuCl_4$ by a solution of sodium borohydride, resulting finally in the formation of a continuous shell of Au.

There has also been research into identifying a core particle onto which Au would nucleate more directly (thereby obviating the need to functionalize it with APS). Some success in this regard has been had with polystyrene latex spheres [63, 64] and silica [64, 65]. Other, related, methods for the synthesis of nanoshells include layer-by-layer deposition to produce polystyrene core/bimetallic (Au-Pd) shells [66], while others [67] have used ultrasonic vibration to coat polystyrene spheres with Ag, Au, Pd and Pt nanocrystals, producing shells of around 0.5 microns diameter. Finally, electroless plating has been used [68] to produce nanoshells with diameters of around 250 nm. While the preceding techniques describe the preparation of a shell with a solid core of some material, yet other reports describe the synthesis of hollow core-shell nanoparticles, for example by using sacrificial templates [31, 55, 56].

In general, however, it is evident that obtaining a reasonable yield of similarly sized nanoshells is not trivial, with all techniques reported to date apparently resulting in a mixture of product forms in comparatively low yields.

### 2.3 Nanorods

#### *2.3.1 Optical properties*

Gold nanorods or ellipsoids (prolate spheroids) provide an alternative to nanoshells for achieving the tunability of the plasmon resonance. The possibilities of ellipsoidal nanoparticles were first recognized by Gans [69] in 1912, who provided an analytical solution for the depolarization factor for ellipsoids of arbitrary aspect ratio; however, there is no general analytical solution for the optical properties of nanorods in general. Nevertheless, it is common to consider them to be ellipsoids (prolate spheroids) e.g.[8, 70-74] and then to model their optical properties using the Gans expression [69]. This predicts that the surface plasmon will split into two modes (longitudinal and transverse) as the aspect ratio of the ellipsoid is increased, with the longitudinal plasmon mode red-shifting significantly and the transverse plasmon blue-shifting slightly [18]. However, real nanorods are more like hemispherically-capped, right cylinders, or like 'dog-bones' or 'dumbbells' [75]. It has been recently found that the end-cap geometry has significant effects on the calculated position of the surface plasmon mode [76, 77]. Here we will model the rods as hemispherically-capped, right cylinders and invoke the DDA to calculate their optical properties directly. Nevertheless, the origins of the mode splitting and dependence on aspect ratio may be understood by consideration of the Gans model, which we will accordingly briefly describe.

The polarizability of an ellipsoid can be described by [2]:

$$\alpha_{x,y,z} = 4\pi abc \frac{\varepsilon_1 - \varepsilon_m}{3\varepsilon_m + 3L_{1,2,3}(\varepsilon_1 - \varepsilon_m)} \quad (10)$$

where *a* is the length of the longitudinal axis and *b* and *c* correspond to the length of the shorter axes. $\varepsilon_1$, $\varepsilon_m$ are the dielectric functions of the spheroid and surrounding medium, respectively and $L_{1,2,3}$ are the geometrical factors. For the prolate spheroid where *a* is the longer axis, *b* = *c*, $L_2 = L_3$ and the applied electric field is parallel to the *x*-axis, Eqn. 10 becomes:

$$\alpha_x = 4\pi abc \frac{\varepsilon_1 - \varepsilon_m}{3\varepsilon_m + 3L_1(\varepsilon_1 - \varepsilon_m)} \quad (11)$$

As was the case with the optical response of the nanoshells, the excitation of the Fröhlich mode follows by setting the denominator of Eqn. 11 equal to zero:

$$3\varepsilon_m + 3L_1(\varepsilon_1 - \varepsilon_m) = 0 \quad (12)$$

This condition is met when:

$$\varepsilon_1 = \varepsilon_m \left(1 - \frac{1}{L_1}\right) \quad (13)$$

where $L_1$ is:

$$L_1 = \frac{1-e^2}{e^2}\left(-1 + \frac{1}{2e}\ln\frac{1+e}{1-e}\right) \quad (14)$$

and $e$ is the eccentricity of the nanorod, which is described by $e^2 = 1 - (\frac{b}{a})^2$. The nanorod polarizability is, once again, directly related to the extinction cross section, $C_{ext}$ by [2, 8] by Eqn. (5). In general, the longitudinal dimension of nanorods exceeds the mean free path of the conduction electrons, so any attenuation effects due to electron scattering are absent for the longitudinal plasmon mode.

The optical response of nanorods can be engineered by changing the geometry and/or the dielectric functions of the nanorod and/or the surrounding medium. The tunability of the surface plasmon modes of nanorods has now been extensively demonstrated experimentally [18, 36, 78-83]. For example Yu *et al.* [78] observed that the longitudinal plasmon peak shifted from 600 to 873 nm as the aspect ratio of their Au nanorods was increased from 1.8 through to 5.2. Murphy and co-workers demonstrated [80] that the longitudinal plasmon resonance could be shifted from 820 nm (aspect ratio of 5 ± 2) to around 1800 – 2200 nm (aspect ratio of 17 ± 3) and then beyond 2200 nm for nanorods with an aspect ratio of 23 ± 4. More recently, multiple higher order plasmon resonances in Au nanorods have also been demonstrated [84].

#### *2.3.2 Synthesis of nanorods*

Silver nanorods were produced in the 1960s using an evaporative shadowing technique [85] and also through the alignment of silver spheres in glass to form pearl necklaces, and have become the mainstay of certain kinds of commercially available dichroic optical filters [86]. The first samples of Au nanorods were synthesized [87-89] in the late 1980s and early 1990s, with both aqueous reduction and the hard template method being used. Interest in nanorods was significantly boosted in 1997 with the discovery of an electrochemical method for rod synthesis by Wang and colleagues [78]. Since then a variety of direct solution-phase synthetic routes have been uncovered and refined [8, 82, 90-99] and the need for an electrochemical cell has been dispensed with. Although the hard template method is still used e.g. [100-104], it appears that the electroless 'seed-mediated' method is now dominant [5, 8].

The seed-mediated synthesis makes use of a 'growth solution', which contains $HAuCl_4$, cetyltrimethylammonium bromide (CTAB) and ascorbic acid, and a 'seed solution' containing very small (~3.5 nm diameter) Au particles. The ascorbic acid within the growth solution is too weak to reduce the $HAuCl_4$ to metallic Au directly in the presence of the CTAB; hence reduction of the $HAuCl_4$ salt occurs almost exclusively on the surface of the seed particles. In the presence of twinned particle seeds, the rod growth occurs along the twin plane, leading to rods with pentagonal cross sections at the peripheries. However, while the mechanism of nanorod growth is still not entirely resolved, control over nanorod aspect ratio, monodispersity and yield can be readily obtained [8, 91]. For example, it has been demonstrated that longer $C_n$ chains in the $C_n$TAB cause an increase in aspect ratio [80], while Jana *et al.* [105] showed that a multi-step seed-mediated synthesis process provides an additional means to control the process, allowing for the production of larger aspect ratio nanorods (13 ± 2 aspect ratio) than those produced by a one-step seed-mediated process (4.6 ± 1 aspect ratio). A high yield (90%) of rods of shorter aspect ratios (up to 4:1) is now routine, facilitated by the addition of small quantities of $Ag^+$ to the growth solution. The silver ions reduce the number of twinned particles and this in turn leads to single crystal Au rods, which grow along the [100] direction and are capped by {110} and {111} facets [90, 105, 106]. The stability of nanorod solutions has been an issue, however. Any unreduced Au in the supernatant solution can precipitate onto the rods over a period of several weeks, causing the end to bulge, and thereby blue shifting the longitudinal plasmon resonance [75]. The problem can be solved by passivating the surface with sodium sulphide [97] or by separating the rods from the gold-bearing supernatant before storage.

In summary, while both Au nanoshells and rods may be prepared by straightforward wet chemical methods, Au rods are more readily prepared on a gram scale and the synthesis appears to be readily scaleable to produce larger quantities.

## 3. Head-to-head

### 3.1 Nanoshells

To enable a 'molar' absorption comparison between rods and shells, the volume of Au used to model each particle was kept

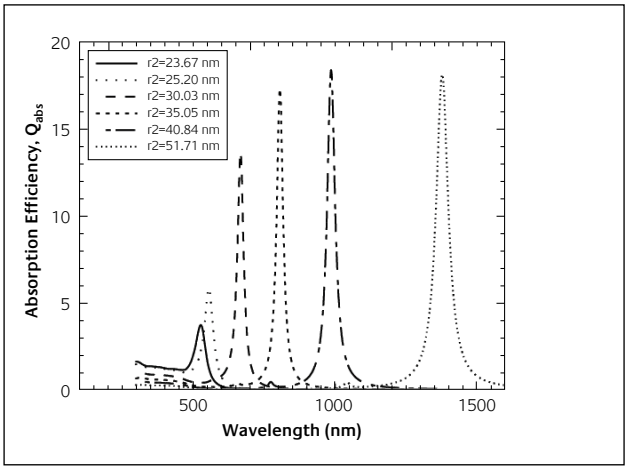


**Figure 2**

*Nanoshell absorption efficiencies for increasing aspect ratios. Note that in this figure any peak heights for a shell of $r_2$>32 nm are likely to be considerably over-estimated due to damping of the plasmons in very thin shells*

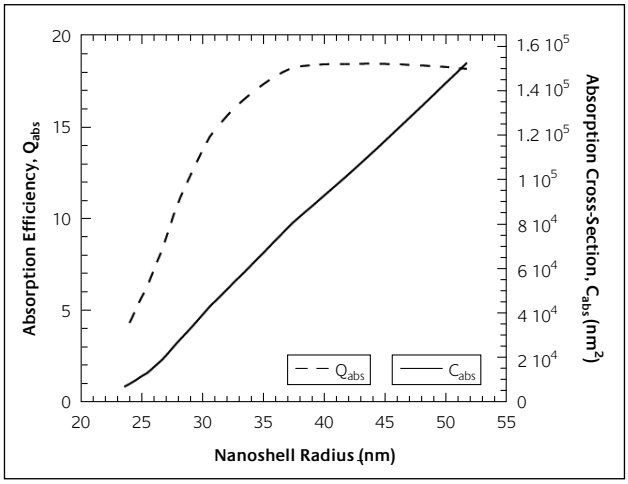


**Figure 3**

*Absorption efficiency and cross-section as a function of nanoshell radius calculated using BHCOAT. Nanoshells were modeled as a shell of fixed volume of Au with a water core with dimensions ranging from $r_1$ = 0 nm, $r_2$ = 23.67 nm to $r_1$ = 50 nm, $r_2$ = 51.71 nm*

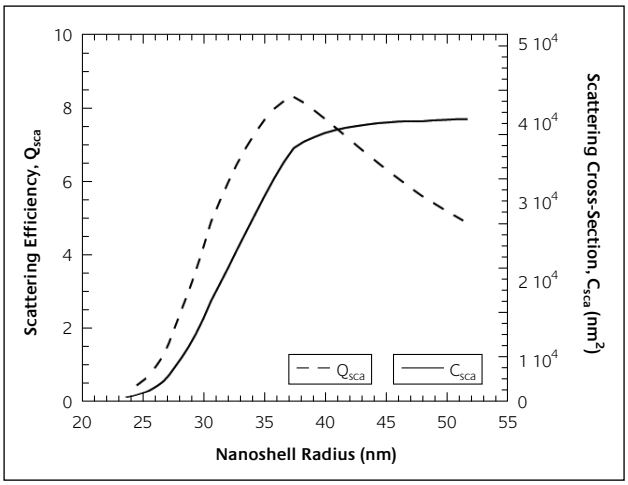


**Figure 4**

*Scattering efficiency and cross-section as a function of nanoshell radius calculated using BHCOAT. Nanoshells modeled as previously described in Figure 3*

constant at 55,550 nm$^3$. This is the same amount contained in a solid Au sphere of 23.7 nm radius. The inner core radius, $r_1$ of the shell (composed of water) was increased in 1 nm steps until a final shell with a radius, $r_2$ of 51.7 nm, shell thickness of 1.7 nm and 0.97 aspect ratio was modeled.

Figure 2 shows the variation in peak absorption efficiency, $Q_{abs}$ as a function of $r_2$. As $r_2$ increases the shell becomes thinner and the aspect ratio increases. This causes the peak $Q_{abs}$ to red-shift from the visible part of the spectrum into the infrared, and to increase in magnitude. For example the solid sphere ($r_2$ = 23.67 nm) produces a maximum $Q_{abs}$ of 3.7 at 530 nm, whereas the shell of 0.97 aspect ratio ($r_2$ = 51.71 nm) ostensibly produces a maximum $Q_{abs}$ of 18.0 at 1380 nm. Note, however, that the bulk dielectric data used would become increasingly inappropriate as the shell thickness decreases below 5 nm, and features on any measured spectrum would be expected to be drastically broadened and attenuated for the thinnest shells, e.g. [27, 107] The physical process may be described in quantum mechanical terms by electron-hole interactions ('Landau damping') [108] or classically as the scattering of the electrons off the surfaces of the shell. For shell thicknesses between 4.8 nm and 1.7 nm, the uncorrected value of $Q_{abs}$ varies between 16 and 18, but here we will take a conservative approach and discount these values. Therefore, the optimum attainable value of $Q_{abs}$ for this volume of Au is probably of the order of no greater than 15, and would be produced by a nanoshell with an outer radius ($r_2$) of about 30 to 32 nm and a shell thickness of 5 or 6 nm.

These extinction cross-sections are of course specific to Au. The intensity of the surface mode is determined by the magnitude of the imaginary component of the material dielectric function: a material with a small imaginary component will have a large, narrow absorption peak whereas a material with a large imaginary component will have a small, broader absorption peak [26].

Figure 3 shows $Q_{abs}$ and absorption cross-section, $C_{abs}$ at the maximum of the plasmon peak plotted against nanoshell radius, $r_2$. In this series of calculations the shell thickness decreases as the diameter increases because the volume of Au used was kept constant. Since, as mentioned, there are factors operating in thin shells that would broaden and attenuate the peak for the thinnest shells, there is also a limit to the extent to which this trend can be reliably projected. The absorption efficiencies of particles with $r_2$>40 nm are likely to be over-estimated here.

Figure 4 shows scattering efficiency, $Q_{sca}$ and scattering cross-section, $C_{sca}$ at the maximum of the plasmon absorption peak, plotted against nanoshell radius, $r_2$. The amount of incident light scattered by the shells is less than the amount they absorb, at the maximum of the plasmon absorption. For example the solid sphere produces a $Q_{abs}$ of 3.71 and a $Q_{sca}$ of 0.25. There is a point reached where $C_{sca}$ becomes relatively constant, which can be seen to occur from shell radii ($r_2$) beyond around 40 nm but this is already in the region where thickness-related errors could be expected. Also, scattering across the entire wavelength spectrum, will increase as the

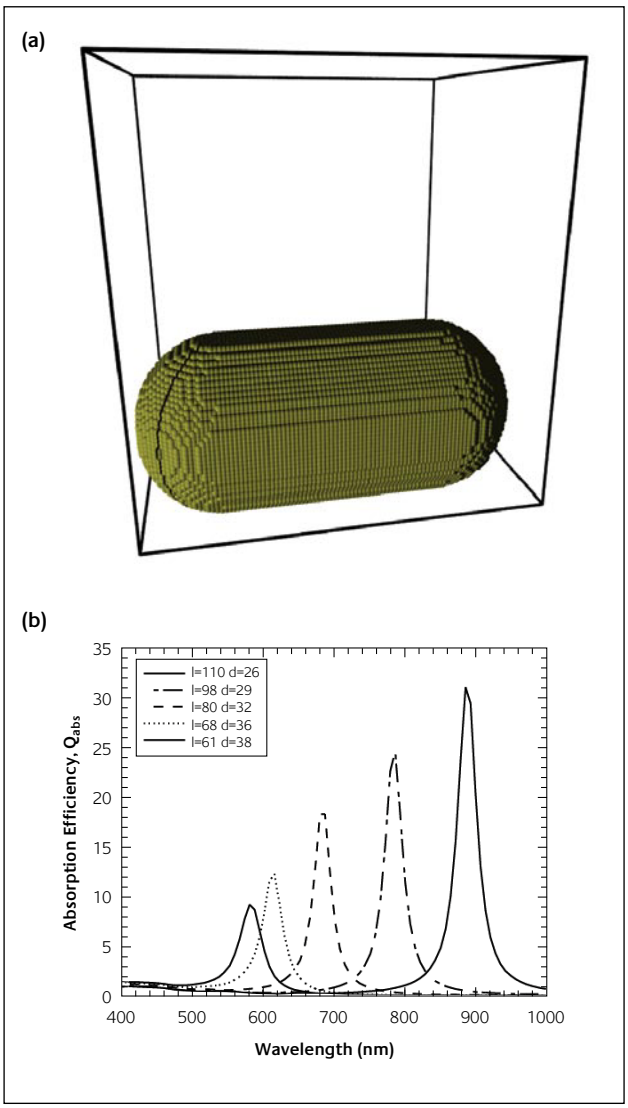


**Figure 5**

*Numerical calculation of the absorption efficiency of Au nanorods of varying aspect ratios: (a) Dipole target used for a rod with l=74 nm and d=33 nm. (b) Nanorod absorption efficiencies for increasing aspect ratios*

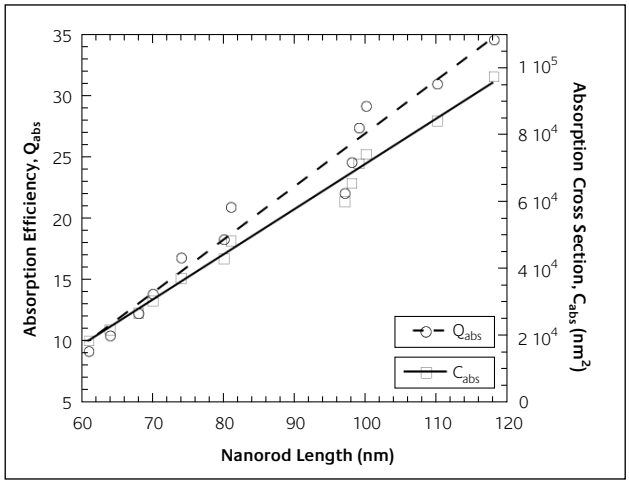


**Figure 6**

*Absorption efficiency and cross-section as a function of nanorod length calculated using DDA. Nanorods were modeled as Au hemispherically capped rods in water with dimensions ranging from l = 61 nm, d = 38 nm to l = 110 nm, d = 26 nm*

particle size increases. These factors strongly impair the spectral selectivity of larger nanoshells, i.e. those with $r_2$>50 nm [59].

### 3.2 Nanorods

Hemispherically-capped, cylindrical nanorods were rendered into a 100 x 100 x 100 point array, but, of course, only a proportion of the sites in this cubic array were actually occupied by Au. The length and diameter of the nanorods were used to determine which of the grid points were "turned on" to represent the nanorod volume. The inter-dipole distance was approximately 1 nm; this ensured that there were sufficient dipoles to accurately represent each nanorod geometry. However, it meant that for some nanorod geometries the actual volume varied slightly from the target volume of 55,550 $nm^3$, with the most extreme case having a tolerance of 55,550 ± 875 $nm^3$ (for the $l$ = 74 nm, $d$ = 33 nm nanorod). Calculations were performed on a number of nanorod geometries with aspect ratios ranging from 1.6 ($l$ = 61 nm, $d$ = 38 nm) to 4.7 ($l$ = 118 nm, $d$ = 25 nm). An example of the dipole target generated for a rod of $l$ = 74 nm is shown in Figure 5(a).

In the case of individual devices made with aligned nanorods it will probably be feasible to ensure that only the longitudinal plasmon resonance is excited ('longitudinal orientation'), however in films or suspensions of randomly oriented rods both resonances must necessarily be excited and the resultant $Q_{abs}$ is a weighted average of the two ('random orientation'). Two intermediate cases arise. In the first the rods are placed in a monolayer on a surface with the long axes in the plane of the surface (a situation relevant to the use of rods in coatings for windows [15], 'planar orientation'), while in the second the rods are aligned with the long axes perpendicular to the surface and parallel to the direction of the incident light ('transverse orientation'). In the planar orientation the resultant $Q_{avg}$ is a simple average of the two resonances, but in the transverse orientation only the transverse resonance will be excited, at least in the case of normally incident light. (Note however that in this case diverse additional and interesting effects, such as dichroism and angular selectivity are possible if the angle of incidence of the light is varied [76].) Each of these cases will be examined here.

Figure 5 (b) shows the variation in longitudinal absorption peak as a function of rod aspect ratio, and it can be seen that the maximum longitudinal $Q_{abs}$ red-shifts with increasing aspect ratio, as predicted by Gans [69]. For example the 1.61 aspect ratio rod produces a peak $Q_{abs}$ of 9.2 at 583 nm, whereas the 4.23 aspect ratio rod produces a peak $Q_{abs}$ of 30.9 at 887 nm. The calculated $Q_{abs}$ and $C_{abs}$ results for nanorods of varying aspect ratio and the longitudinal resonance are shown in Figure 6 for the position of maximum absorption, while Figure 7 shows the calculated scattering efficiency, $Q_{sca}$, and scattering cross-section, $C_{sca}$, for the same nanorods. All of these results are defined in terms of the actual particle cross-section presented to the **k** (propagation) vector of the light. The $Q_{abs}$ values of the transverse resonance

**Table 1**

*$Q_{abs}$ values of an Au nanorod with a volume of 55,500 nm$^3$*

| Aspect ratio | Transverse | Longitudinal | Planar | Random |
|---|---|---|---|---|
| 1.61 | 3.8 | 9.1 | 6.5 | 5.6 |
| 1.89 | 3.8 | 12.2 | 8.0 | 6.6 |
| 2.50 | 4.1 | 18.3 | 11.2 | 8.8 |
| 3.38 | 4.5 | 24.5 | 14.5 | 11.2 |
| 4.23 | 5.2 | 30.9 | 18.1 | 13.8 |

(not shown) are at a similar wavelength and of a similar value to the situation for ordinary nanospheres.

The scatter in the data points within these figures may be explained both by the small errors inherent in the numerical technique and, especially, by the fact that small discontinuities in particle length, radius or volume appear when the nanorod geometries are rendered to a 3-dimensional grid array. Therefore, a line of best fit has been used to fit the data points within each figure.

As described in section 2.3.1, the $C_{abs}$ of the nanorod is influenced by the aspect ratio. This can be seen in Figure 6 where $C_{abs}$ for the longitudinal resonance increases monotonically with increasing nanorod length. The smallest nanorod ($l$ = 61 nm, $d$ = 38 nm) produced a $C_{abs}$ of around 18,350 nm$^2$ and a $Q_{abs}$ of 9.1 at 583 nm. The longest nanorod ($l$ = 118 nm, $d$ = 25 nm) produced a $C_{abs}$ of around 97,130 nm$^2$ and a $Q_{abs}$ of 34.5 at 951 nm. Scattering and absorption showed an upwards linear trend over the range examined, but extrapolation into the untested region of even longer rods should be tempered with caution, as the longitudinal plasmon (and hence $Q_{abs}$) will in practice attenuate for sufficiently long rods because of losses as the plasmon propagates [2]. It can be seen from Figure 7 that $Q_{sca}$ and $C_{sca}$ also increase as the length of the nanorod increases. However, the nanorods still scatter considerably less than they absorb, making them attractive for thermal applications. For example the longest nanorod ($l$ = 118 nm, $d$ = 25 nm) produces a maximum $Q_{abs}$ of 34.5 and $Q_{sca}$ of 18.0, once again in the longitudinal direction.

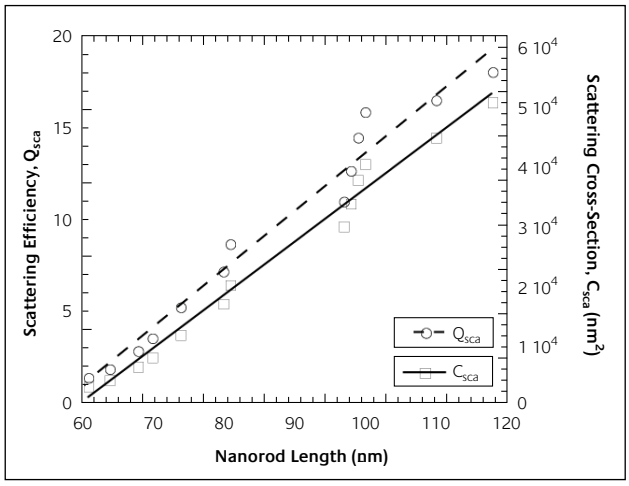


**Figure 7**

*Scattering efficiency and cross-section as a function of nanorod length calculated using DDA. Nanorods were modeled as previously described in Figure 6*

The situation for rods that are aligned in other ways with the electric field of the light is less favorable. In Table 1 we list the applicable $Q_{avg}$ values for rods in the transverse, longitudinal, planar and random orientations. Since the particles all contain the same amount of Au as each other and as the nanoshells discussed earlier, their efficacy can be directly compared. It is apparent that, notwithstanding the positive comments we have made earlier in regard to nanorods, nanoshells are likely to be as good as, or better than, rods for applications, such as hyperthermal medical therapy, that involve randomly oriented particles.

## 4. Conclusions

In the present paper we have compared nanoshells and nanorods containing a common volume of Au. It is clear that the absorption cross-sections of both shapes show a strong, approximately linear, dependence on aspect ratio, but electron scattering effects will tend to attenuate and broaden plasmon peaks in shells with thicknesses less than about 5 nm. This would considerably reduce the efficiency of absorption at a given wavelength. If we place a lower limit of 5 nm on shell thickness, then this implies that (for the given volume of Au), the maximum radius of shell with unimpaired plasmon resonance would be 32 nm, and the corresponding $C_{abs}$ would be ~50,000 nm$^2$. On the other hand, no part of even the longest rods considered here is less than 25 nm in section, and the problems of attenuation and broadening of the plasmon resonances will not manifest themselves. It is clear that rods will always be superior to shells if compared on the basis of longitudinal absorption and equal volumes of Au, but the situation with randomly oriented particles is not as clear-cut, and the two shapes may be equally effective.

## Acknowledgements

This work was supported by the Australian Research Council and AGR Matthey. Computing facilities were provided by the Australian Centre for Advanced Computing and Communication (ac3) in New South Wales, and the National Facility at the Australian Partnership for Advanced Computing (APAC).

## References


1 M. Quinten & U. Kreibig, *Surf. Sci.*, 1986, **172**, 557

2 C. F. Bohren & D. R. Huffman. *Absorption and Scattering of Light by Small Particles* (Wiley, New York, 1998)

3 S. Link & M. A. El-Sayed, *Inter. Rev. Phys. Chem.*, 2000, **19**, 409

4 K. L. Kelly, E. Coronado, L. L. Zhao & G. C. Schatz, *J. Phys. Chem. B*, 2003, **107**, 668

5 C. J. Murphy et al., *J. Phys. Chem. B*, 2005, **109**, 13857

6 C. J. Murphy, A. M. Gole, S. E. Hunyadi & C. J. Orendorff, *Inorg. Chem.*, 2006, **45**, 7544

7 P. Mulvaney, *Langmuir*, 1996, **12**, 788

8 J. Perez-Juste, I. Pastoriza-Santos, L. M. Liz-Marzan & P. Mulvaney, *Coordin. Chem. Rev.*, 2005, **249**, 1870

9 A. Iwakoshi, T. Nanke & T. Kobayashi, *Gold Bull.*, 2005, **38**, 107

10 F. E. Wagner et al., *Nature*, 2000, **407**, 691

11 L. R. Hirsch, J. B. Jackson, A. Lee, N. J. Halas & J. L. West, *Anal. Chem.*, 2003, **75**, 2377

12 I. H. El-Sayed, X. Huang & M. A. El-Sayed, *Nano Lett.*, 2005, **5**, 829

13 R. Elghanian, J. J. Storhoff, R. C. Mucic, R. L. Letsinger & C. A. Mirkin, *Science*, 1997, **277**, 1078

14 X. Xu, M. Stevens & M. B. Cortie, *Chem. Mater.*, 2004, **16**, 2259

15 X. Xu, T. Gibbons & M. B. Cortie, *Gold Bull.*, 2006, **39**, 156

16 K. Aslan, Z. Leonenko, J. R. Lakowicz & C. D. Geddes, *J. Phys. Chem. B*, 2005, **109**, 3157

17 C. Loo et al., *Technol Cancer Res T*, 2004, **3**, 33

18 D. P. O'Neal, L. R. Hirsch, N. J. Halas, J. D. Payne & J. L. West, *Cancer Lett.*, 2004, **209**, 171

19 L. R. Hirsch et al., *Proc. Nat. Acad. Sci. USA*, 2003, **100**, 13549

20 J. L. West & N. J. Halas, *Annu. Rev. Biomed. Eng*, 2003, **5**, 285

21 D. Pissuwan, S. Valenzuela & M. B. Cortie, *Trends Biotechnol.*, 2006, **24**, 62

22 X. Huang, I. H. El-Sayed, W. Qian & M. A. El-Sayed, *J. Am. Chem. Soc.*, 2006, **128**, 2115

23 D. Pissuwan, S. Valenzuela, C. M. Miller & M. B. Cortie, *Nano Lett.*, 2007, in press

24 M.-C. Daniel & D. Astruc, *Chem. Rev.* , 2004, **104**, 293

25 P. K. Jain, K. S. Lee, I. H. El-Sayed & M. A. El-Sayed, *J. Phys. Chem. B.*, 2006, **110**, 7238

26 M. G. Blaber, N. Harris, M. J. Ford & M. B. Cortie. in 2006 International Conference on Nanoscience and Nanotechnology (eds. Jagadish, C.andLu, G. Q. M.) 556 (IEEE Publishing Co, Piscataway, USA, Brisbane, 2006)

27 M. M. Alvarez et al., *J. Phys. Chem. B*, 1997, **101**, 3706

28 M. B. Cortie, A. Dowd, N. Harris & M. J. Ford, *Phys. Rev. B*, 2007, **75**, 113405

29 A. D. McFarland & R. P. Van Duyne, *Nano Lett.*, 2003, **3**, 1057

30 W. R. Glomm, *J. of Dispersion Sci. and Technol.*, 2005, **26**, 389

31 Y. Sun & Y. Xia, *Anal. Chem.*, 2002, **74**, 5297

32 M. G. Blaber, M. D. Arnold, N. Harris, M. J. Ford & M. B. Cortie, *Phys. B*, 2007, **394**, 184

33 Purcell & Pennypacker, *The Astrophysical Journal 186:705-714*, 1973, **186**, 705

34 B. T. Draine & P. J. Flatau, *J. Opt. Soc. Am. A*, 1994, **11**, 1491

35 B. T. Draine & P. J. Flatau, User Guide for the Discrete Dipole Approximation Code DDSCAT 6.1, 2004, http://arxiv.org/abs/astro-ph/0309069

36 A. Brioude, X. C. Jiang & M. P. Pileni, *J. Phys. Chem. B*, 2005, **109**, 13138

37 B. J. Wiley et al., *Nano Lett.*, 2007, **7**, 1032

38 J. H. Weaver & H. P. R. Frederikse. in CRC Handbook of Chemistry and Physics (ed. Lide, D. R.) 12 (CRC Press, Boca Raton, 2001)

39 C. Novo et al., *Phys. Chem. Chem. Phys.*, 2006, **8**, 3540

40 C. Sonnichsen, T. Franzl, T. Wilk, G. v. Plessen & J. Feldmann, *Phys. Rev. Lett.*, 2002, **88**, 077402

41 A. L. Aden & M. Kerker, *J. Applied Phys.*, 1951, **22**, 1242

42 M. Kerker & C. G. Blatchford, *Phys. Rev. B*, 1982, **26**, 4052

43 A. E. Neeves & M. H. Birnboim, *J. Opt. Soc. Am. B* 1989, **6**, 787

44 R. D. Averitt, D. Sarkar & N. J. Halas, *Phys. Rev. Lett.*, 1997, **78**, 4217

45 S. J. Oldenburg, R. D. Averitt, S. L. Westcott & N. J. Halas, *Chem. Phys. Lett.*, 1998, **288**, 243

46 S. J. Oldenburg, J. B. Jackson, S. L. Westcott & N. J. Halas, *Appl. Phys. Lett.*, 1999, **75**, 2897

47 J. L. West, S. R. Sershen, N. J. Halas, S. J. Oldenburg & R. D. Averitt. in US Patent 6,428,811 (USA, 2002)

48 S. J. Oldenburg, R. D. Averitt & N. J. Halas. in US Patent 6,344,272 (2002)

49 J. L. West, N. J. Halas & L. R. Hirsch. in US Patent 6,530,944 (2003)

50 J. L. West, R. Drezek, S. Sershen & N. J. Halas. in US Patent 6,685,730 (2004)

51 E. Prodan & P. Nordlander, *Nano Lett.*, 2003, **3**, 543

52 E. Prodan & P. Nordlander, *J. Chem. Phys.*, 2004, **120**, 5444

53 G. Mie, *Ann. Physik*, 1908, **4**, 377

54 N. Halas, *MRS Bull.*, 2005, **30**, 362

55 H. P. Liang, L. J. Wan, C. L. Bai & L. Jiang, *J. Phys. Chem. B*, 2005, **109**, 7795

56 Z. X. Liu, H. W. Song, L. Yu & L. M. Yang, *Appl. Phys. Lett.*, 2005, **86**, 113109

57 Y. Sun, B. Wiley, Z.-Y. Li & Y. Xia, *J. Am. Chem. Soc.*, 2004, **126**, 9399

58 M. Chen & L. Gao, *Inorg. Chem.*, 2006, **45**, 5145

59 S. Schelm & G. B. Smith, *J. Opt. Soc. Am. A*, 2005, **22**, 1288

60 J. Liu, A. I. Maaroof, L. Wieczorek & M. B. Cortie, *Adv. Mater.*, 2005, **17**, 1276

61 P. Victor et al., *Carbon*, 2006, **44**, 1595

62 H. S. Zhou, I. Honma, H. Komiyama & J. W. Haus, *Phys. Rev. B*, 1994, **50**, 12052

63 K. E. Peceros, X. Xu, S. R. Bulcock & M. B. Cortie, *J. Phys. Chem. B*, 2005, **109**, 21516

64 J. Zhang et al., *Adv. Funct. Mater.*, 2004, **14**, 1089

65 Y. T. Lim, O. O. Park & H.-T. Jung, *J. Colloid Interface Sci.*, 2003, **263**, 449

66 S. Praharaj et al., *Inorg. Chem.*, 2006, **45**, 1439

67 H. A. Atwater, S. Maier, A. Polman, J. A. Dionne & L. Sweatlock, *MRS Bull.*, 2005, **30**, 385

68 D. Suzuki & H. Kawaguchi, *Langmuir*, 2005, **21**, 12016

69 R. Gans, *Annalen der Physik*, 1912, **342**, 881

70 M. Liu & P. Guyot-Sionnest, *J. Phys. Chem. B*, 2004, **108(19)**, 5882

71 C.-D. Chen, Y.-T. Yeh & C. R. C. Wang, *J. Phys. Chem. Solids*, 2001, **62(9-10)**, 1587

72 S. Link, M. B. Mohamed & M. A. El-Sayed, *J. Phys. Chem. B*, 1999, **103**, 3073

73 B. M. I. Van der Zande, L. Pages, R. A. M. Hikmet & A. Van Blaarderen, *J. Phys. Chem. B*, 1999, **103**, 5761

74 K. Ueno, V. Mizeikis, S. Juodkazis, K. Sasaki & H. Misawa, *Opt. Lett.*, 2005, **30**, 2158

75 X. Xu & M. B. Cortie, *Adv. Func. Mater.*, 2006, **16**, 2170

76 M. B. Cortie, X. Xu & M. J. Ford, *Phys. Chem. Chem. Phys.*, 2006, **8**, 3520

77 S. W. Prescott & P. Mulvaney, *J. Appl. Phys.*, 2006, **99**, 123504

78 Y.-Y. Yu, S.-S. Chang, C.-L. Lee & C. R. C. Wang, *J. Phys. Chem. B*, 1997, **101**, 6661
79 A. Gole, C. J. Orendorff & C. J. Murphy, *Langmuir*, 2004, **20**, 7117
80 J. Gao, C. M. Bender & C. J. Murphy, *Langmuir*, 2003, **19**, 9065
81 V. M. Cepak & C. R. Martin, *J. Phys. Chem. B*, 1998, **102**, 9985
82 N. R. Jana, L. A. Gearheart & C. J. Murphy, *J. Phys. Chem. B*, 2001, **105**, 4065
83 S. J. Limmer, T. P. Chou & G. Cao, *J. Phys. Chem. B*, 2003, **107**, 13313
84 B. N. Khlebtsov & N. G. Khlebtsov, *J. Physical Chemistry C, 2007*, in press
85 D. C. Skillman & C. R. Berry, *J Chem. Phys.*, 1968, **487**, 3297
86 anon. (Corning Incorporated, Corning, NY, 2005)
87 M. J. Tierney & C. R. Martin, *J. Phys. Chem.* , 1989, **93**, 2878
88 J. Wiesner & A. Wokaun, *Chem. Phys. Let.*, 1989, **157**, 569
89 C. A. Foss, G. L. Hornyak, J. A. Stockert & C. R. Martin, *J. Phys. Chem.*, 1992, **96**, 7497
90 B. Nikoobakht & M. A. El-Sayed, *Chem. Mater.*, 2003, **15**, 1957
91 J. Perez-Juste, L. M. Liz-Marzan, S. Carnie, D. Y. C. Chan & P. Mulvaney, *Adv. Func. Mater.*, 2004, **14**, 571
92 N. R. Jana, *Small*, 2005, **1**, 875
93 B. D. Busbee, S. O. Obare & C. J. Murphy, *Adv. Mater.*, 2003, **15(5)**, 414
94 T. K. Sau & C. J. Murphy, *Langmuir*, 2004, **20**, 6414
95 A. Gole & C. J. Murphy, *Chem. Mater.*, 2005, **16**, 3633
96 L. Gou & C. J. Murphy, *Chem. Mater.*, 2005, **17**, 3668
97 D. A. Zweifel & A. Wei, *Chem. Mater.*, 2005, **17**, 4256
98 J.-Y. Chang, H. Wu, H. Chen, Y.-C. Lingb & W. Tan, *Chem. Commun.*, 2005, 1092
99 A. J. Mieszawska & F. P. Zamborini, *Chem. Mater.*, 2005, **17**, 3415
100 C. R. Martin *Chem. Mater.*, 1996, **8**, 1739
101 B. M. I. Van der Zande, M. R. Bohmer, L. G. J. Fokkink & C. Schonenberger, *J. Phys. Chem. B*, 1997, **101**, 852
102 B. M. I. van der Zande, M. R. Böhmer, L. G. J. Fokkink & C. Schönenberger, *Langmuir*, 2000, **16**, 451
103 B. Wu & J. J. Boland, *J. Colloid Interface Sci.*, 2006, **303**, 611
104 L. Yang, Q. Y. Cai & Y. Yu, *Inorg. Chem.*, 2006, **45**, 9616
105 N. R. Jana, L. A. Gearheart & C. J. Murphy, *Adv. Mater.*, 2001, **13**, 1389
106 S.-S. Chang, C.-W. Shih & C.-D. Chen, *Langmuir*, 1999, **15**, 701
107 B. Palpant et al., *Phys. Rev. B*, 1998, **57**, 1963
108 C. Yannoulleas, *Annals of Physics*, 1992, **217**, 105